American Journal of Nanosciences
2021; 7(1): 6-14
http://www.sciencepublishinggroup.com/j/ajn
doi: 10.11648/j.ajn.20210701.12
ISSN: 2575-484X (Print); ISSN: 2575-4858 (Online)

Structural, Morphological and Optical Properties of Spray Deposited Multi-doped (Ba, Sr, Mn, Fe and Ni) Compositionally Complex ZnO Thin Films

Mohammad Rahat Al Hassan[1, *], Aungkan Sen[1], Mohammad Khalid Hasan[1], Mohammad Abdul Matin[2]

[1]Department of Glass & Ceramic Engineering, Rajshahi University of Engineering & Technology (RUET), Rajshahi, Bangladesh
[2]Department of Glass & Ceramic Engineering, Bangladesh University of Engineering & Technology (BUET), Dhaka, Bangladesh

Email address:
rahatmme9@gmail.com (M. R. Al Hassan)
[*]Corresponding author

To cite this article:
Mohammad Rahat Al Hassan, Aungkan Sen, Mohammad Khalid Hasan, Mohammad Abdul Matin. Structural, Morphological and Optical Properties of Spray Deposited Multi-doped (Ba, Sr, Mn, Fe and Ni) Compositionally Complex ZnO Thin Films. *American Journal of Nanosciences.* Vol. 7, No. 1, 2021, pp. 6-14. doi: 10.11648/j.ajn.20210701.12

Received: December 21, 2020; **Accepted**: December 31, 2020; **Published**: January 28, 2021

Abstract: Configurational disorder due to high level multi element doping has gained huge attention from research community because of its possibility of unique phase stability as well as unusual functional properties. Based on this context extensive researches performed in recent decades to establish a new horizon of materials i.e. high entropy alloy and ceramics. Of-late, compositionally complex ceramics (CCCs) has been released as an extended form of high entropy ceramics (HECs) where compositional space has been broadened by consideration of both non-equimolecular compositions and relatively low entropy regions. This report aims to stabilize ZnO wurtzite phase at room temperature replacing the Zn-site with five metallic elements i.e. Ba, Sr, Mn, Fe, Ni in equimolecular ratio to impose configurational disorder in the ZnO lattice. Therefore, (BaxSrxMnxFexNix) Zn1-5xO (where x=0, 0.01, 0.02 and 0.03; the films are denoted hereby as ZO, 5DZO, 10DZO and 15DZO respectively) thin films were deposited by low cost spray pyrolysis technique at 200°C. These high-level multi-element doping results in significant effects on the structural, morphological, optical properties of pure ZnO thin film. X-ray diffraction study demonstrated ZnO wurtzite phase stabilization for each deposited film. SEM micrographs revealed a noteworthy transition from original nanorod to well distributed homogeneous fine particles morphology. UV-vis spectroscopy disclosed a sharp rise in transparency (~98%) and band gap (4eV) doped films. At the end, correlations of structural and morphological parameters with tuned functional properties were demonstrated.

Keywords: ZnO, Compositionally Complex Ceramics, Microstructure, Transmittance, Band Gap

1. Introduction

ZnO is one of the most prominent type of semiconducting materials that shows remarkable wide and direct band gap energy of 3.37 eV at room temperature [1]. Therefore, the material is on extensive research focus since the last few decades to make it promising candidate for optoelectronic and photovoltaic applications [2-4]. Diversified film fabrication methods such as:

Laser/plasma-assisted molecular beam epitaxy, CVD, sol-gel, spray pyrolysis, RF/DC sputtering, pulsed laser deposition etc. reported by this time [5, 6]. Furthermore, the variation of dopants type and numbers in the ZnO nanostructure revealed enhanced structural, optical, electrical and magnetic performances of ZnO-based thin films. Also, the fabrication parameters, heat treatment technique etc. play vital role in tuning the ZnO thin film functionalities [6]. However, this study attempts to substitute the Zn-site with five metallic elements i.e. Ba, Sr, Mn, Fe and Ni to obtain stabilized wurtzite ZnO phase with cationic disorder in the microstructure. Hereby, the argument has been introduced taking into account of compositionally complex ceramics (CCCs) synthesis forwarded from the concept of high entropy ceramics (HECs) exposed first by Wright et al [7, 8]. HECs are

defined as mixture of five or more element in equimolecular ratio in at least one cationic sub-lattice of ceramic structure with mixing entropy (ΔS_{mix}) $> 1.60R$ where entropic contribution overcome enthalpic barrier to stabilize structure [9]. But recent researches revealed that entropic stabilization can happened in non-equimolecular mixture as well as in mixture where entropy values are far less than the previously defined value (entropy >1.6R) [10-12]. Wright et al has broadened exclusively the concept of entropy stabilized ceramics from high entropy ceramics to compositionally complex ceramics (CCCs) [7, 8]. Very recently Sen et al also reported compositionally complex BiFeO3 ceramics by incorporation of five different cations in Fe sites, BiFe1–5*x*Mo*x*Ti*x*Zr*x*Ni*x*Ce*x*O3 (x=0.01, 0.02, 0.03) keeping ΔS_{mix} value sharply under 0.69R [13]. Moreover, Miracle et al concluded that there is no hard and fast rule to define the entropy stabilized compounds on the basis of entropy requirement or composition rather than relies on the generation of single-phase structure [14]. Hence, the opportunity of exploring wide compositional space of CCCs group materials boosted this study to synthesize (BaxSrxMnxFexNix) Zn1-5xO thin films. Here five elements have been chosen randomly just on the basis of size variation to impose lattice distortion which is a prominent factor to raise entropy [15]. Besides, transition Metals (TM) i.e. Fe, Mn and Ni were chosen as they have synergistic effects on optoelectronic properties of ZnO. [16, 17]. Films were deposited by spray pyrolysis technique as it is one of the most cost effective, stable and reliable methods to fabricate high quality thin film [18]. Along with structure (X-ray Diffraction) and morphology (SEM), optical properties of the as deposited films were evaluated using UV-vis spectroscopy. The experimental findings are explained later in this report and to the best of our knowledge no such literature has been found yet showing structural stabilization in the low entropy region of compositionally complex ceramics.

2. Experimental Details

2.1. Film Formation

To deposit (ZnO) and (BaxSrxMnxFexNix) Zn1-5xO a simple hand-made spray pyrolysis set up was used in this experiment. ZnO film was synthesized by dissolving analytical grade zinc acetate Zn(CH3COO)2.2H2O (Assay>99%**,** Merck), in deionized water solvent fixing precursor solution concentration of 0.12 M. Similar concentration of precursor solutions were prepared by mixing Zn(CH3COO)2.2H2O, (Assay>99%**,** Merck); Ba(NO3)2**,** (Assay>99%**,** Merck); SrCO3,

(Assay>99%**,** Merck); Mn(NO3)2·4H2O, (Assay>99%**,** Merck); Fe(NO3)3.9H2O, (Assay>99%**,** Merck); Ni(NO3)2·6H2O, (Assay>99%**,** Merck); salts in deionized water to fabricate the 5DZO, 10DZO and 15DZO films. Also, one drop of high concentration HCl **(**Assay>37%**,** Sigma Aldrich) was added in doped samples' solution for complete dissolution. During the experiment, except the solution concentration; the other process parameters were set as: i) substrate temperature: 200°C,

ii) solution flow rate: 0.5 ml/minute and iii) spray outlet to substrate distance: 30cm. Spray were deposited on ultrasonically cleaned and preheated (at 300°C) microscopic glass substrates. The deposited film samples were wrapped in tracing paper and stored for their subsequent characterizations. Several sets of samples were synthesized for each composition and found that their structural, morphological and optical properties could be reproduced.

2.2. Film Characterizations

The structural analysis was conducted by X-Ray diffractometer (Bruker Advanced D8, Germany) for phase identification with Cu wavelength (Kα1=1.54060 Å and Kα2=1.54439 Å). FULLPROF study was performed for structural refinement by Rietveld analysis. Surface morphology was investigated by SEM (ZEISS-EVO 18, UK). Optical transmittance and band gap performance were measured by using UV–vis spectroscopy (Perkin Elmer Lambda 35 UV-Vis spectrophotometer) in the range of 200–800 nm.

3. Result and Discussion

3.1. Structural Study

The X-ray diffraction patterns of the ZO, 5DZO, 10DZO, 15DZO thin films deposited at substrate 200°C are shown in figure 1. All the XRD peaks in all the patterns could be indexed to monophasic zinc oxide hexagonal wurtzite structure according to Joint Committee of Powder Diffraction Standards data (JCPDS card number 36-1451). From the Table 1 it can be noticed that the JCPDS.

Table 1. *XRD data for all the tested samples indexed with JCPDS card number 36-1451 for wurtzite ZnO.*

JCPDS no. 36-1451 ZnO (wurtzite structure)		**ZO**		**5DZO**		**10DZO**		**15DZO**	
2Θ	**hkl**	***2Θ***	**Relative intensity**	***2Θ***	**Relative intensity**	***2Θ***	**Relative intensity**	***2Θ***	**Relative intensity**
31.749	100	31.95	308	31.9	624	31.8	105	31.5	94
34.228	002	34.55	135	34.45	499	34.4	93	34.15	87
36.257	101	36.4	238	36.35	627	36.05	100	36.25	96
47.257	102	47.6	34	47.6	173	47.35	35	47.65	36
	110	56.7	104	56.7	271	56.2	36	56.45	28
	103	66.6	25	66.55	124	66.95	23	66.55	19

ZnO wurtzite crystal's peak positions and spray deposited samples of XRD patterns well match with very negligible dispositioning [19].

The interplaner spacing d_{hkl} increases with dopants addition in the ZnO structure as it proved from Bragg's law of diffraction: 2dhkl sinθ=nλ which implies that the decrement of 2Θ value increase interplaner spacing d. The dhkl for wurtzite structure ZnO unit cell is calculated from the equation.

$$\frac{1}{d^2{}_{hkl}} = \frac{4\,(h^2+hk+k^2)}{3a^2} + \left(\frac{1}{c}\right)^2 \qquad (1)$$

No other extra peak other than ZnO wurtzite structured XRD peaks in all the samples suggests the presence of only one phase of wurtzite ZnO of space group of P 63 mc [20]. Slight dispositioning of doped samples peaks in comparison with ZO ensures complete doping. Moreover, doping occurred from the substitutional replacement of Zn cation (r Zn2+=0.074 nm) by Ba, Sr, Mn, Fe and Ni (rBa2+=0.135 nm, rSr2+=0.118 nm, rMn2+=0.07nm, rFe3+=0.06nm, rNi2+=0.07nm) cations. As large sizes Ba, Sr replace Zn that may result in unit cell volume increment as shown in Table 2.

Table 2. *Structural parameters of ZO, 5DZO, 10DZO & 15DZO thin films obtained by Reitveld refinement, thickness & band gap of the samples.*

Parameters	**Sample**			
	ZO	**5DZO**	**10DZO**	**15DZO**
D (nm)	10.593	9.23	9.34	9.45
a (Å)	*3.238*	*3.243*	*3.256*	*3.258*
c (Å)	*5.204*	*5.207*	*5.206*	*5.218*
c/a	1.607	1.606	1.599	1.602
d100 (Å)	7.863	7.887	7.951	7.96
V (Å^3)	47.29	47.42	47.81	47.95
RZn – Oa (Å)	1.997	2.00	1.99	1.896
RZn – Ob (Å)	1.9675	1.976	1.952	1.896
Ob– Zn– Ob (Degree)	108.00	107.95	108.08	108.00
Ob– Zn– Ob (Degree)	110.90	110.95	110.83	110.9
Strain (ε) *10^{-3}	3.27	3.75	3.71	4.1
Chi^2	1.20	1.38	1.11	1.98
G.o.f	1.1	1.2	1.0	1.4
Rexp	17.8	8.3	17.3	17.5
Film thickness (nm)	69.3	98.6	59.8	91.2
Eg (eV)	3.36	3.95	4.0	3.8

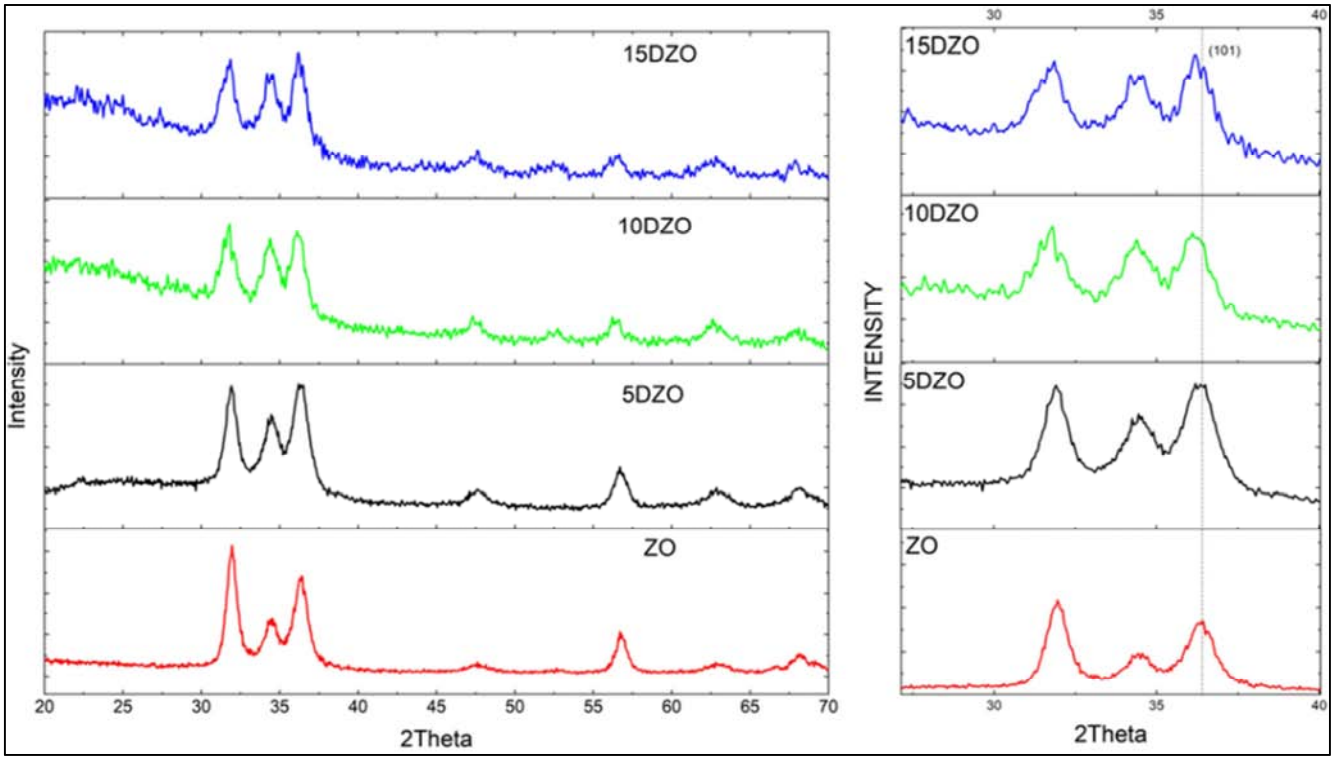

Figure 1. *(a) XRD graphs of ZO, 5DZO, 10DZO, 15 DZO thin film samples (left) and peaks shifting to lower angle (right).*

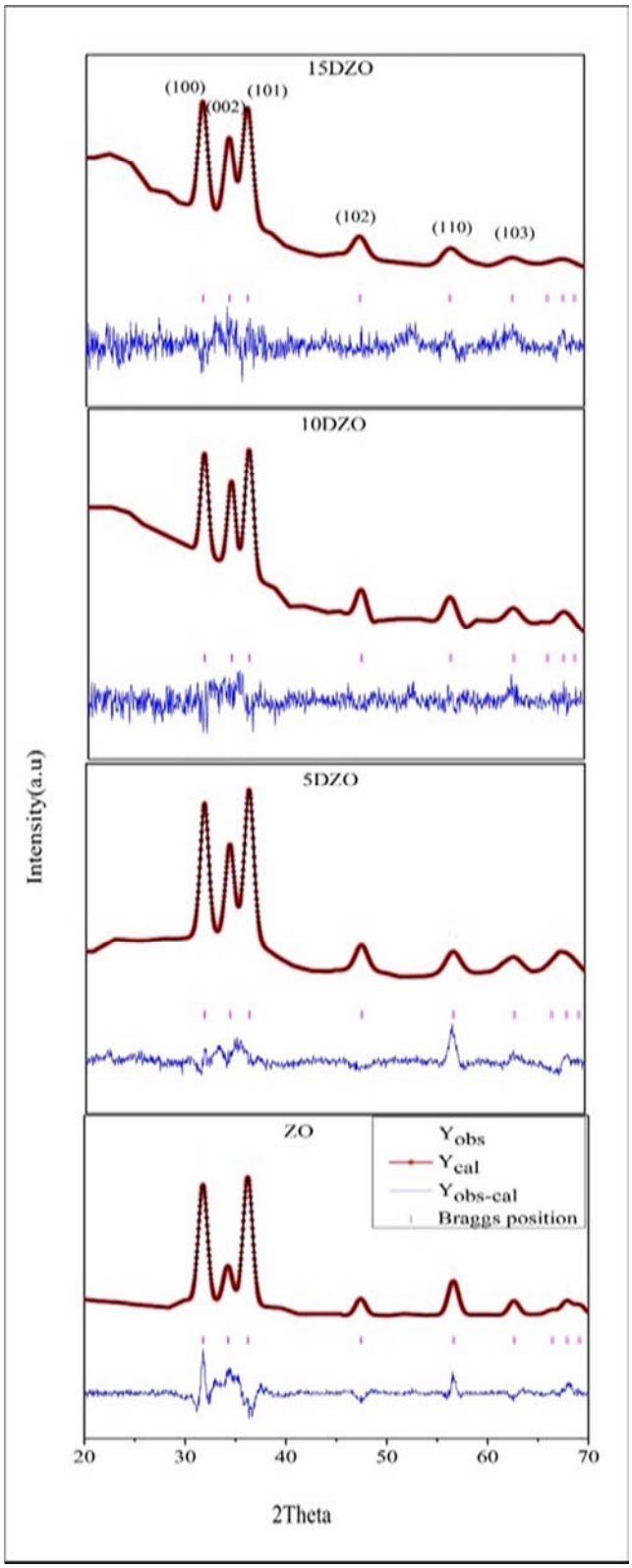

Figure 2. *Reitveld refinement of ZO, 5DZO, 10DZO, 15 DZO samples.*

Full width at half maximum intensity (FWHM), β of (100), (101) and (002) characteristics peaks were utilized in Scherrer equation $D=k\lambda/\beta\cos\theta$, to calculate the average crystallite size, *D* of ZO, 5DZO, 10DZO and 15DZO thin films, where k is the dimensionless constant with a typical value of -0.9, λ is the wavelength of Cu Kα radiation with the value of 1.5418 Å and θ is the Bragg angle. Since with the doping elements addition characteristics XRD peaks broadens shown in figure 2; crystallite size (D) would be decreased. The crystallite size values have been measured as: 10.593, 9.23, 9.34 and 9.45 nm respectively. This can be attributed to the increase of produced nucleation centers due to higher concentration and multi elements doping [21].

Among all the samples improved crystalline properties of 5DZO samples as diffraction intensities of all peaks enhanced than ZO samples and preferred growth orientation changed from (100) plane in to (002) plane in 5DZO, 10DZO and 15DZO samples. This c-axis preferential growth may result from an easy crystal growth due to highest atomic planer density along (002) [22]. As with higher doping of 10 and 15%, peaks intensity falls down with high background noise which indicates reducing crystallinity and inducing stress. Highly induced stress in 10DZO, 15DZO films also may be attributed to the change in O-Zn-O angle and Zn-O bond length values. Annealed stress released samples may show improved crystallinity [23].

To investigate the changes in crystal structure and parameters, Reitveld refinement of the synthesized samples was carried out using FULLPROF Suite program as shown in figure 2. The XRD pattern shows that the deposited samples have hexagonal wurtzite structure belonging to the space group of P63mc [20]. The refined structural parameters of the synthesized thin film samples are enlisted in following Table 2.

The refined lattice parameters (a & c) values demonstrate the effect of doping as it is clearly noticed that larger size Ba, Sr doping increase unit cell parameters and accordingly the cell volumes as tabulated below. To summarize, the XRD patterns of ZO, 5DZO, 10DZO and 15DZO samples well match with single phase ZnO crystal with wurtzite-type structure and hexagonal phase (P 63 mc space group).

3.2. Morphological Study

Surface morphological studies of ZO, 5DZO, 10DZO and 15DZO films were carried out from scanning electron micrographs (SEM). Figure 3 (a-d) shows the SEM images of all the undoped and doped ZnO thin films. The micrographs indicate that, during deposition of ZnO and doped ZnO by spraying the solution onto heated substrates, the growth has taken place by nucleation and coalescence process.

Both spherical and rod like textures of grains were observed in ZO film surface morphology. This nano rod texture may be due to particle agglomeration effect. But in all the doped samples this morphology changed to flakes like appearance. Such type of morphology well match with the report of Deshpande's work of ZnO spray deposited thin film [24]. The size distribution of nanorod and flake-like particles' diameter is depicted utilizing linear intercept method through histogram graph as in figure 4 [25]. It is evident from SEM micrographs and histogram chart that dopant addition in ZnO structure significantly reduces the particle size. This particle

size reduction may be due to the effect of dopant (Ba, Sr, Mn, Fe and Ni) atoms influence in rising nucleation sites and lattice distortion; thus, hindered the growth process resulting into the formation of smaller grains.

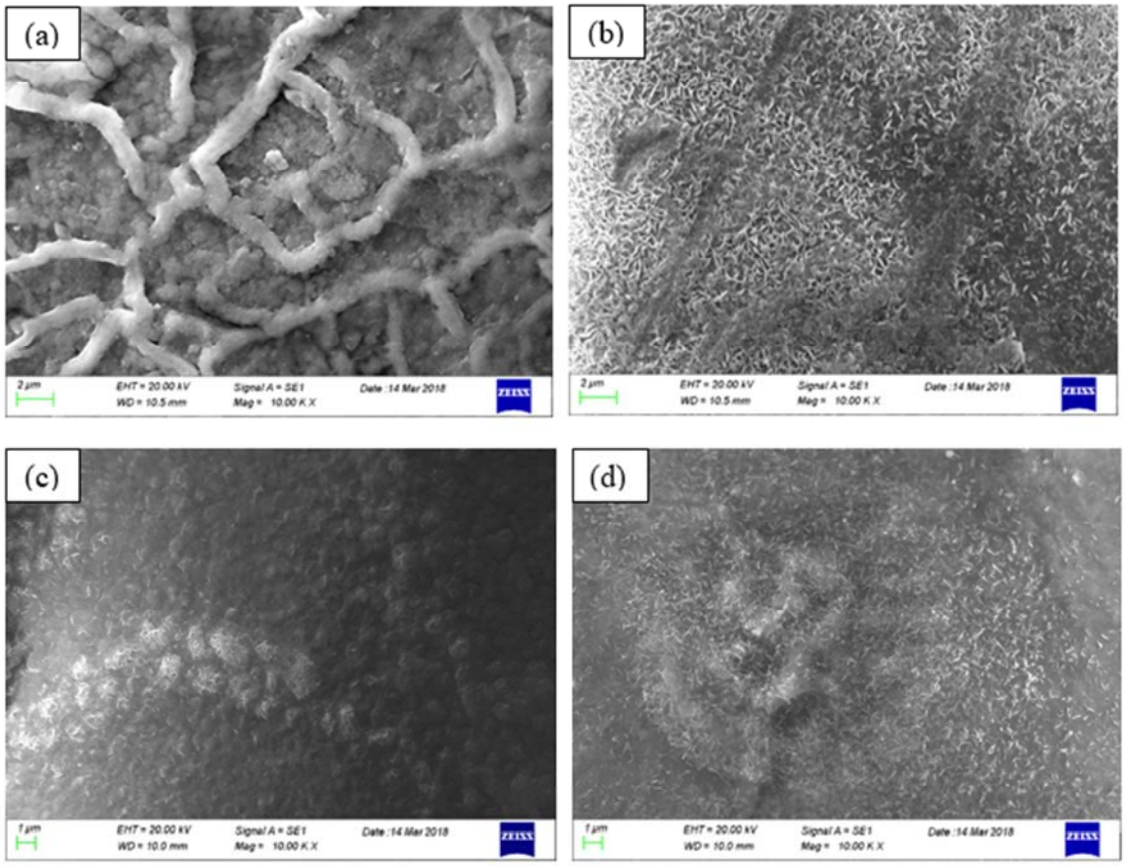

Figure 3. *Scanning Electron micrographs (SEM) at 10,000X of (a) ZO, (b) 5DZO, (c) 10DZO and (d) 15DZO.*

3.3. Optical Study

Optical transmission spectroscopy results of all the samples has been shown in figure 5 keeping wavelength range of 200–800 nm. The transmission is found to be maximum for 5DZO film sample about 98% in 780-790 nm wavelengths and then decreased for 10DZO and 15DZO film gradually. The surface morphology of 5DZO films is more coherent, smooth and well-crystalized than other films' surface. Therefore, 5DZO shows highest transmittance performance due to less light scattering and it can be exclusively used for window layers in solar cells [26]. Then for higher dopants in ZnO the surface texture changed towards enhanced roughness, voids presence, lattice distortion and enhanced residual stress as noticed in SEM micrographs and XRD results. Hence, increased scattering of photons by crystal defects in 10DZO and 15DZO films may be attributed in the reduction of optical transmittance [27, 28]. Besides, defects in the microstructure influence strongly the transmittance of the film and the argument aligns with the study of Sun et al [29].

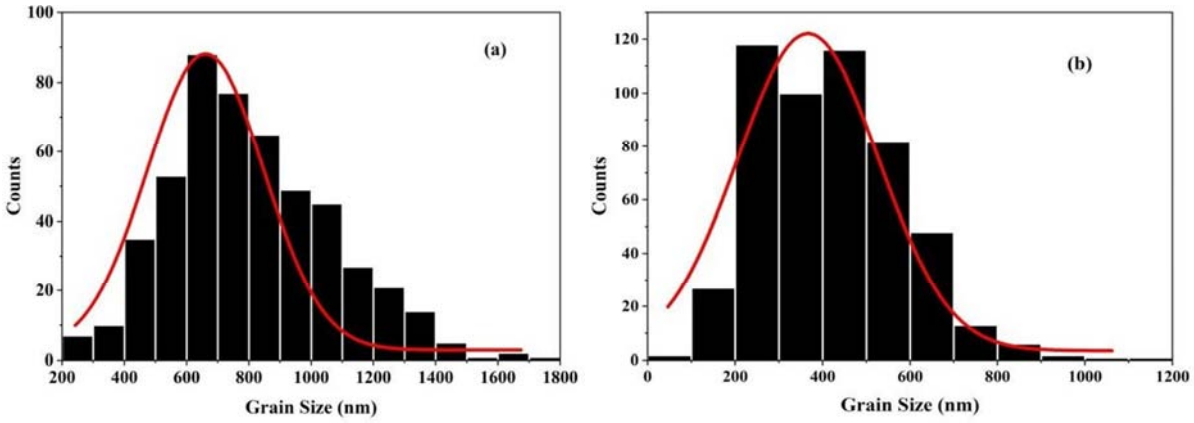

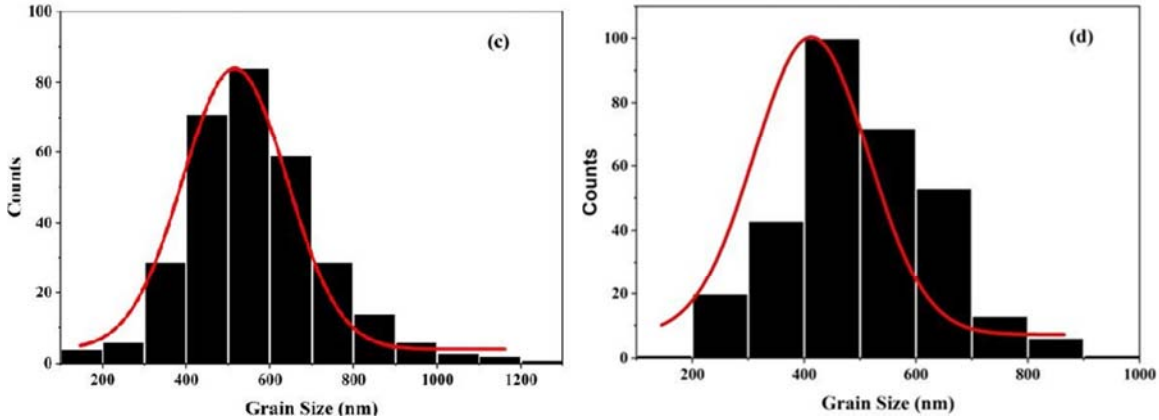

Figure 4. *Histograms of (a) ZO (b) 5DZO (c) 10DZO and (d) 15DZO samples regarding particle size distribution.*

A characteristic difference in the absorption edge was observed with dopants incorporation in ZnO. A sharp absorption edge has been observed for ZO at around 380 nm. As dopant concentration increased, significant blue shifting of absorption edge has been observed towards the lower wavelength at 290 to 300 nm range for 5DZO and 10DZO films as shown in figure 6. These shifting are considered as the indicator of enhanced band gap for doped film samples. It was found that the absorbance initially decreased sharply and then decreased gradually for all the samples in the visible range. The decrease in absorbance with doping may be attributed to the decrease in the size of nanoparticles which ultimately widens the bandgap [30].

Film thickness can be measured from optical reflectance data. If n_1 and n_2 are the refractive indices at two adjacent reflectance maxima (or minima) at the wavelength λ_1 and λ_2, respectively, then by Swanepoels method [31] film thickness d can be measured from the following equation.

$$d = \frac{\lambda_1 \lambda_2}{2(n_1\lambda_2 + n_2\lambda_1)} \quad (2)$$

The determined film thickness of all the samples has been enlisted in the Table 2. The optical band gap (Eg) for the deposited films was calculated on the basis of spectral absorption for ZnO type direct band gap material using the Tauc's relation as follows:

$$\alpha h\upsilon = (h\upsilon - Eg)^{\frac{1}{2}} \quad (3)$$

Where $h\upsilon$ is the incident photon energy, A is constant and hence the band gap has been calculated by extrapolating the linear region of the plots $(\alpha h\upsilon)^2$ versus $h\upsilon$ on the energy axis as shown in figure 7 (a-d). The optical band gap of material depends on many properties like thickness, defects, absorption co-efficient and type of materials [32]. The material with high band gap is useful for solar cell application [33].

The optical band gap significantly increased for 5DZO, 10DZO and 15DZO films (Eg=3.95, 4.0 and 3.8 eV respectively) compared to ZO (3.36 eV). Such widening of optical band gap with multi- element doping where an enhancement of n type carrier concentration occurred in ZnO structure due to (Fe^{3+} doping) can be well described by Burstein–Moss effect [33-35]. By enhancement of n type carrier concentration with doping; absorption edge forms at much shorter wavelengths than intrinsic samples and lowers the Fermi level down into the conduction band which widens band gap. This is the well-known as Burstein–Moss effect.

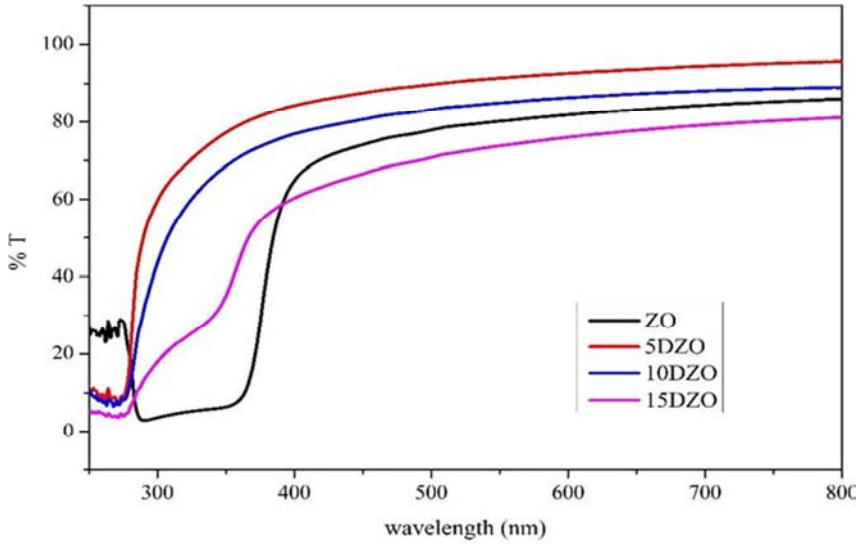

Figure 5. *UV-vis transmission spectrum of ZO, 5DZO, 10DZO and 15DZO films.*

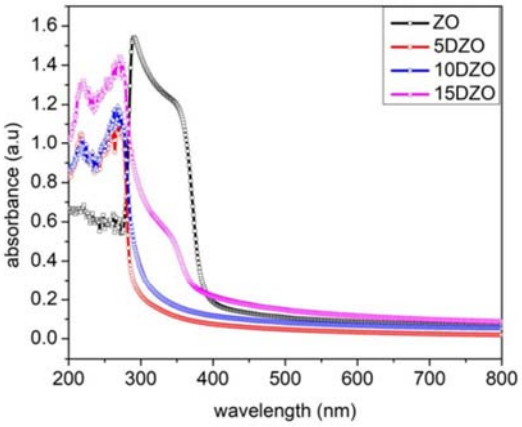

Figure 6. *UV-vis absorbance spectrum of ZO, 5DZO, 10DZO and 15DZO films.*

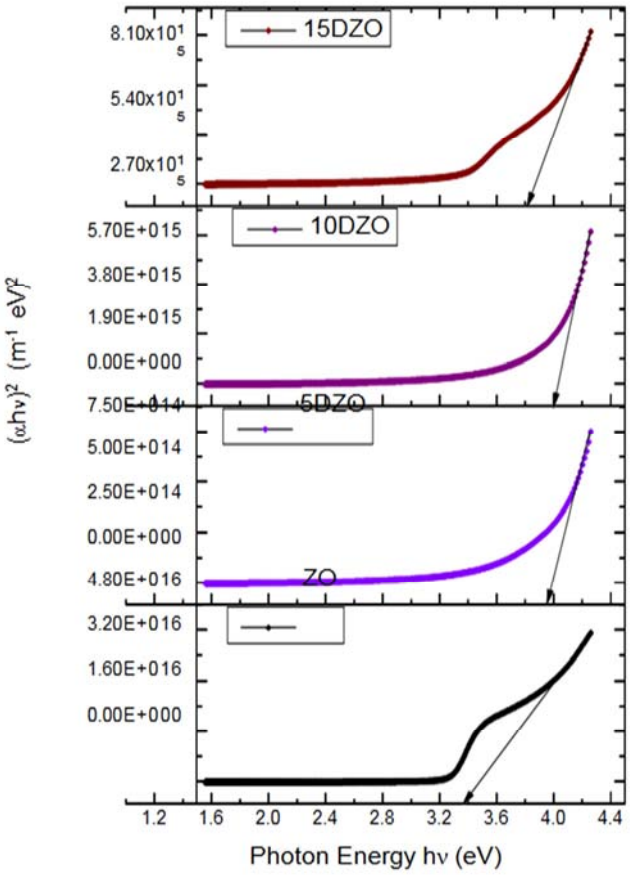

Figure 7. *Plot of $(\alpha\, h\upsilon)^2$ versus incident photon energy ($h\upsilon$) for (a) ZO, (b) 5DZO, (c) 10DZO and (d) 15DZO films.*

The refractive index and extinction coefficient of these films were determined using transmittance and reflectance measurements. Figure 8 shows the refractive index spectrum of both doped and undoped samples. The refractive index, (n) has been calculated using the relation [36].

$$n = \frac{(1+R)}{(1-R)} + \sqrt{\frac{4R}{(1-R)^2 - K^2}} \qquad (4)$$

As well as, refractive index is found to decrease with the addition of Ba, Sr, Mn, Fe and Ni dopants. This may be due to the change in crystallite size, stoichiometry and internal strain with the addition of various sizes dopants to the Zn-O network [37, 38]. It has been observed that an overall decreasing trend for the refractive index with the photon energy shifting to the higher value that is towards the lower value of wave length. It has been found for all the samples that an overall increase in the refractive index towards the larger wavelength in the visible region.

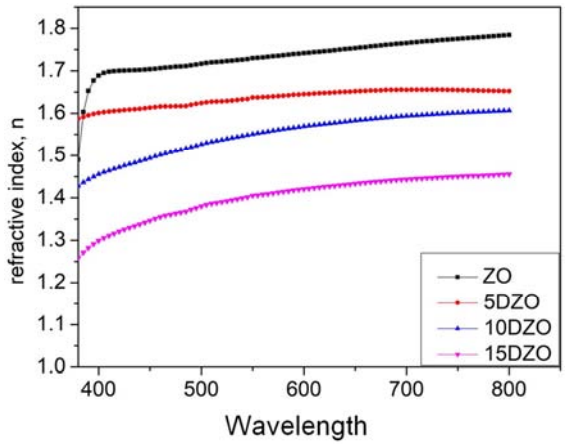

Figure 8. *Refractive index versus wavelength for ZO, 5DZO, 10DZO and 15DZO films.*

4. Conclusion

This experiment highlights the effects of five elements equimolecular ratio doping on the structural, morphological and optical characteristics of pure and doped (BaxSrxMnxFexNix) Zn1- 5xO (where x=0, 0.01, 0.02 and 0.03) spray deposited thin films. As the multi-component (BaxSrxMnxFexNix) Zn1-5xO structure for the first time ever reported in literature; easier and effective synthesis route selection was a crucial issue to proceed the work. To meet this challenge, selection of spray pyrolysis method for film deposition is appropriate as multiple dopants penetration into the lattice is easier in this method. No impurity phase presence in the XRD data interprets ZnO wurtzite phase lattice formation with multiple dopants in the structure. Single ZnO wurtzite phase stabilization even for high concentration doping in 15DZO film is evidence of entropic influence in the nanostructure. In addition, sluggish diffusion phenomenon in crystal growth stage due to multicomponent doping effects is supposed to be another factor in single phase stabilization of ZnO class CCCs. Afterwards, the comparative structural analysis showed good crystallinity, homogeneous flake and nanowire shaped particles were found in 5DZO compared with other films from XRD and SEM results. Very good optical transparency, band gap widening and increased optical conductivity were noticed in doped samples; especially in 5DZO film (%T=98, E_g=4.0 eV). This composition has vast potentiality to be employed in semiconductor that could be operated at much higher

voltages, frequencies and temperatures other than conventional Si-based semiconducting material. Though for higher doping transmittance value decreased, conduction of post annealing after film deposition might retain higher transmittance level. To conclude, the wide compositional space of CCCs needs to be extensively explored yet to open the possibilities of establishing noble category materials of supreme structural and functional properties in this context.

Conflict of Interest

The authors declare that they have no competing interests.

Acknowledgements

The authors would like to thank the Rajshahi University of Engineering & Technology (RUET) and the Bangladesh University of Engineering & Technology (BUET) for providing necessary testing facilities.

References

[1] Srinivasulu, T., Saritha, K., & Reddy, K. R. (2017). Synthesis and characterization of Fe- doped ZnO thin films deposited by chemical spray pyrolysis. *Modern Electronic Materials*, *3* (2), 76-85.

[2] Guo, X. L., Choi, J. H., Tabata, H., & Kawai, T. (2001). Fabrication and optoelectronic properties of a transparent ZnO homostructural light-emitting diode. *Japanese Journal of Applied Physics*, *40* (3A), L177.

[3] Drici, A., Djeteli, G., Tchangbedji, G., Derouiche, H., Jondo, K., Napo, K.,. & Gbagba, M. (2004). Structured ZnO thin films grown by chemical bath deposition for photovoltaic applications. *physica status solidi (a)*, *201* (7), 1528-1536.

[4] Chu, J. B., Huang, S. M., Zhang, D. W., Bian, Z. Q., Li, X. D., Sun, Z., & Yin, X. J. (2009). Nanostructured ZnO thin films by chemical bath deposition inábasic aqueous ammonia solutions for photovoltaic applications. *Applied Physics A*, *95* (3), 849-855.

[5] Jiao, S., Lu, Y., Zhang, Z., Li, B., Yao, B., Zhang, J., & Fan, X. (2007). Optical and electrical properties of highly nitrogen-doped ZnO thin films grown by plasma-assisted molecular beam epitaxy. *Journal of Applied Physics*, *102* (11), 113509.

[6] Mozammel, M., Ilkhechi, N. N., Tanouraghaj, E. F., & Rezaei, E. (2019). Evaluation of the effect of high concentration of dopant (Cr, Sn) on structural, optical, and wettability properties of ZnO thin films. *Journal of the Australian Ceramic Society*, *55* (4), 999-1007.

[7] Wright, A. J., Wang, Q., Huang, C., Nieto, A., Chen, R., & Luo, J. (2020). From High- Entropy Ceramics to Compositionally-Complex Ceramics: A Case Study of Fluorite Oxides. *Journal of the European Ceramic Society*.

[8] Wright, A. J., & Luo, J. (2020). A step forward from high-entropy ceramics to compositionally complex ceramics: a new perspective. *Journal of Materials Science*, 1-16.

[9] Rost, C. M., Sachet, E., Borman, T., Moballegh, A., Dickey, E. C., Hou, D. & Maria, J. P. (2015). Entropy-stabilized oxides. *Nature communications*, *6*, 8485.

[10] Djenadic, R., Sarkar, A., Clemens, O., Loho, C., Botros, M., Chakravadhanula, V. S., & Hahn, H. (2017). Multicomponent equiatomic rare earth oxides. *Materials Research Letters*, *5* (2), 102-109.

[11] Zhang, Y., Zuo, T. T., Tang, Z., Gao, M. C., Dahmen, K. A., Liaw, P. K., & Lu, Z. P. (2014). Microstructures and properties of high-entropy alloys. *Progress in Materials Science*, *61*, 1-93.

[12] Jien-Wei, Y. E. H. (2006). Recent progress in high entropy alloys. *Ann. Chim. Sci. Mat*, *31* (6), 633-648.

[13] Sen, A., Hasan, M. K., Munna, A. H., Roy, D. J., Al Hassan, M. R., & Gulshan, F. (2020). Structural, optical, and magnetic properties of compositionally complex bismuth ferrite (BiFeO 3). *Journal of Materials Science: Materials in Electronics*, 1-15.

[14] Miracle, D. B., & Senkov, O. N. (2017). A critical review of high entropy alloys and related concepts. *Acta Materialia*, *122*, 448-511.

[15] Yeh, J. W. (2013). Alloy design strategies and future trends in high-entropy alloys. *Jom*, *65* (12), 1759-1771.

[16] Rajalakshmi, R., & Angappane, S. (2013). Synthesis, characterization and photoresponse study of undoped and transition metal (Co, Ni, Mn) doped ZnO thin films. *Materials Science and Engineering: B*, *178* (16), 1068-1075.

[17] Soitah, T. N., Chunhui, Y., & Liang, S. (2010). Effect of Fe doping on structural and electrical properties of nanocrystalline ZnO thin films prepared by sol–gel dip coating technique. *Science of Advanced Materials*, *2* (4), 534-538.

[18] Filipovic, L., Selberherr, S., Mutinati, G. C., Brunet, E., Steinhauer, S., Köck, A., & Schrank, F. (2014). Methods of simulating thin film deposition using spray pyrolysis techniques. *Microelectronic Engineering*, *117*, 57-66.

[19] Etape, E. P., Foba-Tendo, J., Ngolui, L. J., Namondo, B. V., Yollande, F. C., & Nguimezong, M. B. N. (2018). Structural Characterization and Magnetic Properties of Undoped and Ti-Doped ZnO Nanoparticles Prepared by Modified Oxalate Route. *Journal of Nanomaterials*, *2018*.

[20] Kumar, S., Asokan, K., Singh, R. K., Chatterjee, S., Kanjilal, D., & Ghosh, A. K. (2014). Investigations on structural and optical properties of ZnO and ZnO: Co nanoparticles under dense electronic excitations. *RSC Advances*, *4* (107), 62123-62131.

[21] Mahmood, K., & Park, S. B. (2013). Atmospheric pressure based electrostatic spray deposition of transparent conductive ZnO and Al-doped ZnO (AZO) thin films: effects of Al doping and annealing treatment. *Electronic Materials Letters*, *9* (2), 161-170.

[22] Amirhaghi, S., Craciun, V., Craciun, D., Elders, J., & Boyd, I. W. (1994). Low temperature growth of highly transparent c-axis oriented ZnO thin films by pulsed laser deposition. *Microelectronic engineering*, *25* (2-4), 321-326.

[23] Lee, Y. C., Hu, S. Y., Water, W., Tiong, K. K., Feng, Z. C., Chen, Y. T., & Cheng, M. H. (2009). Rapid thermal annealing effects on the structural and optical properties of ZnO films deposited on Si substrates. *Journal of Luminescence*, *129* (2), 148-152.

[24] V. P. Deshpande, S. D. Sartale, A. N. Vyas, A. U. Ubale, Temperature Dependent Properties of Spray Deposited Nanostructured ZnO Thin Films, *International Journal of Materials and Chemistry*, Vol. 7 No. 2, 2017, pp. 36-46

[25] Sen, A., Niloy, K. H., Islam, Z., Al Hassan, M. R., Zaman, T., Abdul, M. M., & Gulshan, F. (2020). Influence of Ba and Mo co-doping on the structural, electrical, magnetic and optical properties of BiFeO 3 ceramics. *Materials Research Express*.

[26] Reddy, N. N. K., Akkera, H. S., Sekhar, M. C., & Park, S. H. (2017). Zr-doped SnO 2 thin films synthesized by spray pyrolysis technique for barrier layers in solar cells. *Applied Physics A*, *123* (12), 761.

[27] Rajpure, K. Y., Lokhande, C. D. and Bhosale, C. H., 1999. A comparative study of the properties of spray-deposited Sb2Se3 thin films prepared from aqueous and nonaqueous media. *Materials research bulletin*, *34* (7), pp. 1079-1087.

[28] Kumar, P. R., Kartha, C. S., Vijayakumar, K. P., Abe, T., Kashiwaba, Y., Singh, F. and Avasthi, D. K., 2004. On the properties of indium doped ZnO thin films. *Semiconductor science and technology*, *20* (2), p. 120.

[29] Sun, R. D., Nakajima, A., Fujishima, A., Watanabe, T. and Hashimoto, K., 2001. Photoinduced surface wettability conversion of ZnO and TiO2 thin films. *The Journal of Physical Chemistry B*, *105* (10), pp. 1984-1990.

[30] Rahdar, A. (2013). Effect of 2-mercaptoethanol as capping agent on ZnS nanoparticles: structural and optical characterization. *Journal of Nanostructure in Chemistry*, *3* (1), 10.

[31] Swanepoel, R. (1983). Determination of the thickness and optical constants of amorphous silicon. *Journal of Physics E: Scientific Instruments*, *16* (12), 1214.

[32] Zeng, H., Duan, G., Li, Y., Yang, S., Xu, X. and Cai, W., 2010. Blue Luminescence of ZnO nanoparticles based on non-equilibrium processes: defect origins and emission controls. *Advanced Functional Materials*, *20* (4), pp. 561-572.

[33] Sernelius, B. E., Berggren, K. F., Jin, Z. C., Hamberg, I. and Granqvist, C. G., 1988. Band- gap tailoring of ZnO by means of heavy Al doping. *Physical Review B*, *37* (17), p. 10244.

[34] Moss, T. S. (1954). The interpretation of the properties of indium antimonide. *Proceedings of the Physical Society. Section B*, *67* (10), p775.

[35] Mondal, S. B. S. R., Bhattacharyya, S. R., & Mitra, P. (2013). Effect of Al doping on microstructure and optical band gap of ZnO thin film synthesized by successive ion layer adsorption and reaction. *Pramana*, *80* (2), p315-326.

[36] Gadallah, A. S. and El-Nahass, M. M., 2013. Structural, optical constants and photoluminescence of ZnO thin films grown by sol-gel spin coating. *Advances in Condensed Matter Physics*, *2013*.

[37] Tepehan, F., & Özer, N. (1993). A simple method for the determination of the optical constants, n and k of cadmium sulfide films from transmittance measurements. *Solar energy materials and solar cells*, *30* (4), 353-365.

[38] Ashour, A., El-Kadry, N., & Mahmoud, S. A. (1995). On the electrical and optical properties of CdS films thermally deposited by a modified source. *Thin solid films*, *269* (1-2), 117-120.